

# Modelling subsonic turbulence with SPH-EXA

Rubén Cabezón  
University of Basel  
Basel, Switzerland  
ruben.cabezón@unibas.ch

Domingo García-Senz  
Polytechnic University of Catalonia  
Barcelona, Spain

Osman Seckin Simsek  
University of Basel  
Basel, Switzerland

Sebastian Keller  
Swiss National Supercomputing Center  
Lugano, Switzerland

Axel Sanz  
Polytechnic University of Catalonia  
Barcelona, Spain

Yiqing Zhu  
University of Basel  
Basel, Switzerland

Lucio Mayer  
University of Zürich  
Zürich, Switzerland

Ralf Klessen  
University of Heidelberg  
Heidelberg, Germany

Florina M. Ciorba  
University of Basel  
Basel, Switzerland

**Abstract**—The numerical simulation of subsonic turbulence with SPH has traditionally been hindered by E0 errors, inaccurate gradient evaluations, and excessive dissipation. In this work, we present numerical results of SPH simulations of subsonic turbulence and compare to state-of-the-art codes such as AREPO and GIZMO. For the first time, SPH can reproduce the results of such codes, showing a similar interval of wavenumber in the inertial range of the Kolmogorov cascade in the subsonic regime. We use the SPH-EXA code to perform these simulations, a GPU-based state-of-the-art SPH code with high performance and extreme scalability at its core. SPH-EXA is coupled with a modern SPH solver based on methods such as an integral approach to gradient calculation, artificial viscosity switches that include a linear field cleaner, a flexible family of pairing-resistant interpolation kernels, generalized volume elements, and a controlled handling of density jumps which maximizes Lagrangian compatibility. In addition, it includes a novel and extremely scalable gravity solver for astrophysical applications.

## I. INTRODUCTION

Smoothed Particle Hydrodynamics (SPH) is a very flexible and adaptable numerical technique for solving partial differential equations in continuum mechanics that has been successfully applied in many different fields. In particular, its application in fluid dynamics, solid mechanics, and astrophysics has substantially benefited those respective fields since its conception around year 1980 [1, 2]. At the core of its success lay its excellent conservation properties, the lack of an underlying structured mesh, and its natural treatment of three-dimensional calculations [3, 4, 5]. Despite these considerable advantages, SPH has historically struggled with certain types of calculation. In particular, those related to the development of subsonic turbulence.

Turbulence is a fundamental multiscale phenomenon in fluid dynamics, characterized by chaotic and unpredictable fluid flow [6]. It occurs in both natural environments and technological applications, making its study and understanding crucial across various fields of science and engineering. Turbulence plays a vital role in the formation and evolution of astronomical structures, from accretion disks around black holes to the large-scale structure of the universe. It influences the distribution of galaxies, star formation, and the dynamics of the interstellar medium. In meteorology, turbulence

affects weather patterns, cloud formation, and the dispersion of pollutants. Understanding turbulence is essential for accurate weather forecasting, climate modeling, and assessing environmental impacts. Ocean currents exhibit turbulent behavior, affecting marine ecosystems, climate systems (through heat and carbon exchange), and navigation. Turbulence also plays a role in phenomena such as El Niño and the mixing of nutrients from deep waters to the surface. In aerospace, automotive, and chemical engineering, controlling or exploiting turbulence can lead to more efficient designs. For example, reducing turbulence around aircraft wings or vehicle bodies can reduce fuel consumption and emissions. In contrast, enhancing turbulence in reactors can improve mixing and chemical reactions. Turbulence challenges our understanding of nonlinear dynamical systems and fluid mechanics. It is a rich field for theoretical and computational research, seeking universal laws and models to describe turbulent flows. Despite its ubiquity and importance, turbulence remains one of the most challenging areas of physics to model and predict due to its complex, non-linear nature. Progress in this field beyond the heuristic but very successful pioneering model by Kolmogorov [7] can lead to advances in technology, improved environmental management, and deeper insights into the fundamental processes of nature.

The numerical simulation of turbulence has been a very powerful tool to progress in its understanding, yet such simulations are very challenging as they require to be accurate across a vast range of scales for very long simulation times. This implies high-resolution simulations with state-of-the-art codes. In general, there are no significant discrepancies between simulations with SPH and with grid-based methods for supersonic turbulence [8]. Nevertheless, reproducing subsonic or transonic turbulence with SPH has been traditionally a challenge because it failed to produce results with sufficient quality to compete with grid-based methods for a similar resolution [9]. First studies of subsonic turbulence with SPH in the context of cosmological simulations [10, 11] which found a rough agreement with the Kolmogorov power spectra but only in a very limited range of wavenumbers. More recent attempts to simulate turbulence by direct numerical simulation (DNS) only led to minor [9] or moderate improvements [12], with

the latter highlighting the importance of reducing the viscosity away from shocks. However, the velocity power spectra still showed significant differences with those obtained with mesh-based calculations. All these studies identified zeroth order,  $E0$ , errors, excessive dissipation, and inaccurate estimation of gradients as the principal causes of the difficulties in simulating turbulence with SPH at low-Mach numbers.

Adapting Large Eddy Simulation (LES) concepts to SPH was shown to be a promising route to simulating turbulence [13, 14] although at the price of introducing additional, and somehow artificial, terms in the basic SPH formulation with a loss in the Lagrangian compatibility of the method. On another note, there is little doubt that DNS simulations of subsonic turbulence would benefit from a better estimation of gradients, [15], e.g. by using an integral approach (IA) to derivatives [16] to obtain a better agreement with the Kolmogorov power spectra and in a wider range of wavelengths.

In this work, we present SPH simulations of subsonic turbulence calculated with the SPH-EXA code, a state-of-the-art, highly scalable hydrodynamic code that incorporates the latest improvements in High-performance Computing (HPC), such as full GPU porting of the SPH computation kernels, efficient domain decomposition, GPU-based neighbor search, on-the-fly initial conditions generation, and in-situ visualization. It also incorporates the latest improvements in the SPH technique such as the mentioned IA to calculate gradients, generalized volume elements, optimized Lagrangian compatibility [17, 18] and an efficient linear field cleaner [19] among others. Equipped with such a bag of resources we show that the simulations of turbulence with SPH-EXA can compete with those obtained with top reference codes such as GIZMO [20] and AREPO [21]. Our results reproduce an increasing inertial range of the Kolmogorov cascade with resolution, which, thanks to the excellent scaling properties of SPH-EXA, will make an increasingly larger fraction of the inertial range of turbulence accessible to DNS in the forthcoming years.

## II. METHODOLOGY

### A. Gradients

SPH-EXA implements an integral approach to calculate derivatives [16, 22].

The IA formalism calculates gradients of an arbitrary function  $f$  by solving the following matrix equation:

$$\begin{bmatrix} \partial f / \partial x_1 \\ \partial f / \partial x_2 \\ \partial f / \partial x_3 \end{bmatrix}_a = \begin{bmatrix} \tau_{11} & \tau_{12} & \tau_{13} \\ \tau_{21} & \tau_{22} & \tau_{23} \\ \tau_{31} & \tau_{32} & \tau_{33} \end{bmatrix}_a^{-1} \begin{bmatrix} I_1 \\ I_2 \\ I_3 \end{bmatrix}_a, \quad (1)$$

where the  $\tau$  tensor elements are defined as:

$$\tau_{ij,a} = \sum_b V_b (x_{i,b} - x_{i,a})(x_{j,b} - x_{j,a}) W_{ab}(h_a); \quad i, j = 1, 3. \quad (2)$$

Here  $x_i$  is the vector position coordinates,  $V_b$  the volume element,  $W_{ab}$  the interpolation kernel, and  $I_{i,a}$  the vector integral elements, which are calculated as:

$$I_{i,a} = \left[ \sum_b V_b f_b (x_{i,b} - x_{i,a}) W_{ab}(h_a) \right]; \quad i = 1, 3. \quad (3)$$

As a consequence, the gradients calculation is:

$$\nabla_i f_a = \sum_b V_b (f_b - f_a) A_{i,ab}(h_a); \quad i = 1, 3 \quad (4)$$

where,

$$A_{i,ab}(h_a) = \sum_{j=1}^3 c_{ij,a}(h_a)(x_{j,b} - x_{j,a}) W_{ab}(h_a) \quad (5)$$

where the summation is up to 3 for 3D simulations and  $c_{ij,a}$  the elements of the inverse of matrix  $\mathcal{T}$ , that is,  $\mathcal{C} = \mathcal{T}^{-1}$  (Eq. 1).

### B. Artificial Viscosity

The basic AV implementation in SPH-EXA is the following:

$$\Pi_{ab}^{AV} = \begin{cases} -\frac{\alpha}{2} v_{ab}^{sig} w_{ab} & \text{for } \mathbf{x}_{ab} \cdot \mathbf{v}_{ab} < 0 \\ 0 & \text{otherwise} \end{cases}, \quad (6)$$

where  $\alpha$  is the viscous parameter and is usually set to 1. The signal velocity estimator between a pair of particles is:

$$v_{ab}^{sig} = \frac{1}{2} (c_a + c_b) - 2w_{ab}, \quad (7)$$

Finally,  $c_a$  and  $c_b$  are the local speed of sound for each particle, and  $w_{ab} = (\mathbf{v}_{ab} \cdot \mathbf{x}_{ab}) / |\mathbf{x}_{ab}|$ .

A linear velocity field implies a smooth flow without the presence of shocks. Therefore, linear velocity fields should have a vanishing AV. We reconstruct the local velocity field for each particle by removing the linear component of the velocity jump that is used to trigger and calculate the AV in Eq. 6 [19]. Assuming that it is differentiable in the neighborhood of each SPH particle, the best linear approximation of the velocity field is given by multiplying its Jacobian by the distance to its neighbors. Instead of using  $\mathbf{v}_{ab} = \mathbf{v}_a - \mathbf{v}_b$  to calculating  $w_{ab}$ , we use  $\mathbf{v}'_{ab} = \mathbf{v}'_a - \mathbf{v}'_b$ , defined as:

$$v'_{a,i} \equiv v_{a,i} - \frac{1}{2} \phi_{ab} \mathbf{J}_{\mathbf{v}_a} \mathbf{x}_{ab}^T \quad (8)$$

$$v'_{b,i} \equiv v_{b,i} + \frac{1}{2} \phi_{ba} \mathbf{J}_{\mathbf{v}_b} \mathbf{x}_{ab}^T \quad (9)$$

where  $\mathbf{x}_{ab}^T = \mathbf{x}_a - \mathbf{x}_b$  is the column vector of relative distance and  $\mathbf{J}_{\mathbf{v}}$  is the Jacobian of the velocity field. In the case of the presence of discontinuities, such a linear estimator is not accurate enough; hence, the  $\phi_{ab}$  factor is designed to go to zero in these cases, while it is kept close to 1 when the field is smooth. To this end, we use a van Leer-like limiter [19]:

$$\phi_{ab} = \max \left[ 0, \min \left( 1, \frac{4F_{ab}}{(1+F_{ab})^2} \right) \right] \times \kappa_{ab}, \quad (10)$$

$$\kappa_{ab} \equiv \begin{cases} \exp \left[ - \left( \frac{q_{ab} - q_{crit}}{q_{fold}} \right)^2 \right] & \text{if } q_{ab} < q_{crit}, \\ 1 & \text{if } q_{ab} \geq q_{crit}, \end{cases} \quad (11)$$

$$q_{ab} \equiv \min(q_a, q_b), \quad (12)$$

$$q_{crit} \equiv \left( \frac{32\pi}{3nb_a} \right)^{1/3}, \quad (13)$$

$$F_{ab} \equiv \frac{\mathbf{x}_{ab} \mathbf{J}_{\mathbf{v}_a} \mathbf{x}_{ab}^T}{\mathbf{x}_{ab} \mathbf{J}_{\mathbf{v}_b} \mathbf{x}_{ab}^T}, \quad (14)$$

where  $q_a$  is the normalized distance between neighbors ( $q_a = |\mathbf{x}_b - \mathbf{x}_a|/h_a$ ),  $q_{crit}$  is the average of the interparticle distance normalized to the smoothing length in 3D, and  $nb_a$  is the number of neighbors of particle  $a$ . The parameter  $q_{fold}$  determines the width of the correction factor  $\kappa_{ab}$  (Eq. 11) that is applied to the van Leer limiter (Eq. 10) and we use the recommended value [19] of  $q_{fold} = 0.2$ .

The final step is to effectively control excessive dissipation. This can be done by allowing a dynamic individual viscous parameter  $\alpha_a$  in Eq. 6, rather than having a constant value for all SPH particles. Several methods have been developed to calculate  $\alpha_a$ , but the nominal works of [23] and [24] are the inspiration behind our implementation in SPH-EXA. The main idea is that  $\alpha_a$  should be initialized by default at a rather low value (usually  $\alpha_a = 0.05$ ). Then it increases rapidly if dissipation is needed and decays exponentially to its original value when it is not needed, effectively acting as a switch for the AV at the position of each SPH particle.

We start by calculating a local viscous parameter  $\alpha_{loc,a}$ , following the definition [23]:

$$\alpha_{loc,a} = \begin{cases} \frac{\alpha_{max} \mathcal{D}_a}{\mathcal{D}_a + h_a |\nabla \cdot \mathbf{v}_a| + 0.05c_a} & \text{for } \nabla \cdot \mathbf{v}_a < 0, \\ 0 & \text{otherwise,} \end{cases} \quad (15)$$

where  $\mathcal{D}_a = h_a^2 |\nabla(\nabla \cdot \mathbf{v}_a)|$  predicts flow convergence by comparing the gradient of  $\nabla \cdot \mathbf{v}_a$  with the local value of  $\nabla \cdot \mathbf{v}_a$ . If the former is large enough and the fluid is actually converging ( $\nabla \cdot \mathbf{v}_a < 0$ ),  $\alpha_{loc,a}$  adopts a value between 0 and  $\alpha_{max}$ . Furthermore, the term  $0.05c_a$ , where  $c_a$  stands for the local speed of sound, acts as a base value for the size of the velocity fluctuations that can trigger dissipation, and it also works as a term to prevent divergent  $\alpha_{loc,a}$ .

Once we know  $\alpha_{loc,a}$  we have two options:

- if  $\alpha_{loc,a} \geq \alpha_a$ : we instantaneously rise the dissipation setting  $\alpha_a = \alpha_{loc,a}$ ,
- if  $\alpha_{loc,a} < \alpha_a$ : we let  $\alpha_a$  decay smoothly.

In the case that  $\alpha_a$  has to decay, we evaluate an instantaneous decay rate  $\dot{\alpha}_a$  as in [23]:

$$\dot{\alpha}_a = \begin{cases} (\alpha_{loc,a} - \alpha_a)/\tau_a & \text{if } \alpha_{min} < \alpha_{loc,a} < \alpha_a, \\ (\alpha_{min} - \alpha_a)/\tau_a & \text{if } \alpha_{min} \geq \alpha_{loc,a}. \end{cases} \quad (16)$$

The decay time  $\tau_a$  is defined as  $\tau_a = h_a/v_{sig,max}$ , and it is a function of the local spatial resolution and the maximum signal velocity  $v_{sig,max}$  in the neighborhood of particle  $a$ , calculated according to Eq. 7. The effect of Eq. 16 is to allow alpha to decay exponentially to  $\alpha_{loc,a}$ , or  $\alpha_{min}$  if  $\alpha_{loc,a}$  is too low. In this way, we ensure a minimum dissipation that helps reduce the random noise that might arise from particle disorder. However, we note that even though all particles have at least a minimum value  $\alpha_{min}$ , dissipation is automatically cut off when  $\mathbf{r}_{ab} \cdot \mathbf{v}_{ab} \geq 0$ , as stated in Eq. 6. Also, there is no restriction for  $\alpha_{min}$ , which can be set to zero.

### C. Volume elements

In the context of SPH, where we are discretizing the SPH integral interpolant, it becomes necessary to compute the volume element that corresponds to each particle. An uncomplicated yet highly effective method is  $dx'^3 \equiv V_b \sim m_b/\rho_b$ . However, it is known [25, 26] that the discretization of the volume element, present in most SPH equations, can be improved beyond this classical approximation using generalized volume elements (GVE).

GVE are usually expressed as:

$$V_a = \frac{X_a}{\sum_{b=1}^{nb} X_b W_{ab}}, \quad (17)$$

where  $X$  is an arbitrary function. In SPH-EXA we adopted the GVE described in the work of [18], which has shown to provide a better treatment of discontinuities, stronger resistance to tensile instability, better partition of unity, and more accurate gradient evaluation:

$$X_a = \frac{m_a}{\rho_a^0}, \quad (18)$$

where  $\rho_a^0 = \sum_b m_b W_{ab}$  is the standard SPH density calculation. With Eqs. 17 and 18 we can simply calculate the particle density as  $\rho_a = m_a/V_a$ .

### D. Lagrangian compatibility

One of the most common artifacts in SPH simulations is tensile instability, which can, in some cases, prevent mixing and the development of hydrodynamical instabilities. Several approaches have been developed to deal with such problems [25, 27, 28], all of which require a departure to some extent from the pure Lagrangian formulation. In SPH-EXA we adopted a novel implementation [18], which, to our knowledge, is currently the only adaptive method that sacrifices Lagrangian compatibility *exclusively* in regions of the fluid at (and adjacent to) contact interphases, improving the accuracy at those regions, in turn. Hence, we define a self-adaptive parameter that is individual to each particle-neighbor pair as follows:

$$\sigma_{ab} \equiv \begin{cases} 0 & \text{if } At_{ab} \leq At_{min}, \\ R(At_{ab} - At_{min}) & \text{if } At_{min} \leq At_{ab} \leq At_{max}, \\ 1 & \text{if } At_{ab} \geq At_{max}, \end{cases} \quad (19)$$

with  $R = (At_{max} - At_{min})^{-1}$  and  $At_{ab}$  is the pairwise Atwood number, defined as  $At_{ab} = \left| \frac{\rho_a - \rho_b}{\rho_a + \rho_b} \right|$ . We use the values  $At_{max} = 0.2$  and  $At_{min} = 0.1$ , as suggested in [18]. In this implementation  $0 \leq \sigma \leq 1$  (see Eqs. 22 and 23). In particular, when  $\sigma = 0$  the resulting SPH equations are fully Lagrangian, while  $\sigma = 1$  leads to a version less Lagrangian compatible but more tensile resistant. The parameter  $\sigma$  appears in the momentum and energy SPH equations and has the effect of crossing and uncrossing the particle and neighbor's magnitudes.

### E. Interpolation kernel

We use the sinc family ( $S_n$ ) [29, 30] as interpolation kernels,

$$W_{ab} = S_n = \frac{K}{h_a^d} \begin{cases} 1 & q_a = 0 \\ \left[ \text{sinc} \left( \frac{\pi}{2} q_a \right) \right]^n & q_a \leq 2 \\ 0 & q_a > 2 \end{cases} \quad (20)$$

where  $K$  is a normalization constant,  $h$  is the smoothing length,  $d$  is the spatial dimension,  $q_a$  is the normalized distance between neighbor particles ( $q_a = |\mathbf{x}_b - \mathbf{x}_a|/h_a$ ), and  $n$  is a user-defined real value that makes the kernel more centrally peaked as it increases. Usually  $3 < n < 9$ . It is known [31] that a necessary condition for an SPH kernel to avoid pairing instability is that its Fourier transform is definite positive. As such, they proposed the use of Wendland functions [32] as SPH kernels. These have been adopted by many researchers for this reason. The other side of the coin is that Wendland kernels need a large number of neighbors to perform accurate interpolations, which leads to considerable computational efforts. A possible alternative is to use pairing-resistant kernels. Despite not having an always positive Fourier transform, they are constructed to have small negative Fourier regions and push them to large wavenumbers. This allows these kernels to use a lower number of neighbors than Wendland functions, while still suppressing pairing instability. Sinc kernels are an example of such kernels. The simulations reported in this work were calculated choosing  $n = 6$  in Eq. 20.

### F. SPH-EXA hydrodynamic equations

The final set of hydrodynamic equations in SPH-EXA is as follows:

$$\rho_a = m_a/V_a, \quad (21)$$

$$\frac{dv_{i,a}}{dt} = - \sum_b m_b \times \left[ \frac{X_a^{2-\sigma} X_b^\sigma P_a}{\Omega_a m_a^2 k_a} A_{i,ab}(h_a) + \frac{X_b^{2-\sigma} X_a^\sigma P_b}{\Omega_b m_b^2 k_b} A_{i,ab}(h_b) \right], \quad (22)$$

$$\frac{du_a}{dt} = \frac{X_a^{2-\sigma} P_a}{m_a^2 \Omega_a k_a} \sum_b \sum_{i=1}^d m_b X_b^\sigma [(\mathbf{v}_a - \mathbf{v}_b) \cdot \mathbf{A}_{ab}(h_a)] + \left( \frac{du_a}{dt} \right)^{AV}. \quad (23)$$

Here  $P_a$  is the pressure,  $X_a = m_a/\rho_a^0$  the selected function for the GVE,  $k_a$  the normalization of the GVE ( $k_a \equiv \sum_b X_b W_{ab}$  in Eq. 17),  $A_{i,ab}(h_a)$  the IA term, and  $\Omega_a$  the grad-h term. The parameter  $\sigma$  controls how close the implementation is to a pure Lagrangian scheme (as discussed above). The last term in the energy equation includes the contributions of artificial viscosity.

### G. Initial conditions

We have designed an embedded initial conditions (IC) generator in SPH-EXA. In all our tests, we use a template of a relaxed box with  $50^3$  particles. This box has previously been relaxed to achieve a glass-like configuration [33] with constant density and periodic boundary conditions. Replicating this box in different directions allows us to create on-the-fly initial conditions with a user-defined number of particles and in a distributed manner, only limited by the memory of the system. In this way, ICs can be scaled up just by changing one input argument and without the need to store large files, ensuring reproducibility and simplifying the process of performing suites of tests at scale.

All simulations presented here were performed on a box of side  $L = 1$ , periodic boundary conditions, initial density  $\rho = 1$ , and 'quasi'-isothermal equation of state with an adiabatic index  $\gamma = 1.001$ . The fluid is stirred using the Ornstein-Uhlenbeck process [34, 35] following a parabolic amplitude field  $\sim 1 - (k - k_c)^2$ , with  $k = |\mathbf{k}|$ , and  $k_c = 2$ , which corresponds to a length  $L/2$ , and vanishing for  $k \leq 1$  and  $k \geq 3$ . This approach is implemented to reduce the impact of the stirring on the energy cascade, facilitating a natural transfer of energy from larger to smaller scales. We also use a natural mixing of 1/3 compressive and 2/3 solenoidal contributions. All simulations start in a homogenous state and are stirred for a total of  $t = 10$ , until they reach the stationary state<sup>1</sup> with an RMS Mach number of  $M = 0.3$ .

## III. RESULTS

To evaluate the weight and significance of the different elements that contribute to our SPH implementation, we conducted identical simulations while progressively incorporating more of these elements. Figure 1 shows the power spectrum of the velocity field of simulations of  $250^3$  particles with increasing complexity, compared to the S3 simulation of [9] with  $256^3$  particles and the classic SPH formulation (i.e. gradients calculated directly as kernel derivatives, no GVEs, and no viscosity switches), labeled STD in our plot.

The inclusion of IA recovers the correct slope in the inertial range of the Kolmogorov cascade for smaller wavenumbers, considerably extending it compared to STD, but is not enough to affect the classical excessive slope of  $\sim -4$  at large wavenumbers. At these small scales something else is needed. The inclusion of GVE and artificial viscosity switches (labeled as VAV in Fig. 1 provides a step in the right direction.

<sup>1</sup>All our times are normalized with the sound-crossing time, which in our setup is  $t_{sc} = L/c = 1$ .

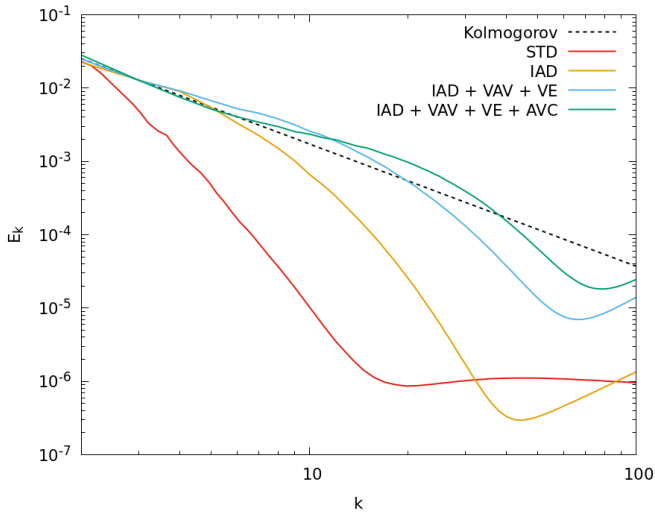


Fig. 1. Comparison of the power spectra of the velocity field for  $M = 0.3$  with different elements incorporated into the SPH solver. The dashed line is the theoretical Kolmogorov power spectrum of  $\sim k^{-5/3}$ . STD stands for standard SPH and is taken from [9] (simulation S3 in their Fig. 6, with  $256^3$  particles). All other simulations were performed with SPH-EXA and  $250^3$  particles. IA stands for including the integral formalism to calculate derivatives. VAV stands for variable AV and implies the inclusion of AV switches. GVE is for generalized volume elements, and AVC for AV cleaning. All these elements have been described in Sec. II.

With these elements, we start to see the bottleneck effect as the excess of energy at increasing wavenumber, commonly encountered close to the resolution limit in mesh-based simulations. Finally, the inclusion of the artificial viscosity cleaner (AVC in Fig. 1) provides the final push, extending the inertial range almost a decade with respect STD, showing the bottleneck effect clearly, and having a slope in the dissipative regime similar to those of non-Lagrangian codes (see Fig. 4).

Figure 2 presents the power spectrum of the velocity field for simulations performed with SPH-EXA and with different particle counts at the end of each simulation ( $t = 10$ ). It is clear that with increasing resolution, the inertial range over the Kolmogorov scale is extended to larger wavenumber, and more importantly, that the rate of enhancement with increasing number of particles is not marginal or small, but considerable and consistent with that obtained with modern mesh-based and moving-mesh methods. This is a novel result, which means that SPH can indeed resolve smaller scales with higher resolution, in opposition to the results found with older SPH implementations by [9]. Figure 3 shows a thin slice of the velocity field for increasing resolution with SPH-EXA, from  $200^3$  up to  $3000^3$ , where it is evident how we can resolve a delicate and rich mixture of large- and small-scale features.

Now we can directly compare our results with other state-of-the-art codes that are not purely Lagrangian. Figure 4 displays a comparison of the power spectra calculated with AREPO, GIZMO, and SPH-EXA. As can be seen, SPH-EXA is able to reproduce the same inertial range. We can also see the bottleneck effect to a very similar extent in all three codes.

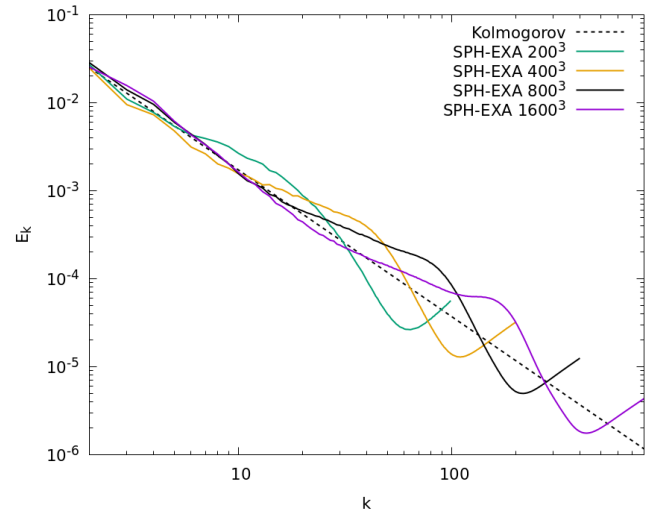


Fig. 2. Comparison of the power spectra of the velocity field at  $t = 10$  for  $M = 0.3$  at increasing resolution. Each line corresponds to an increase of a factor 2 in resolution with respect to the previous curve.

As this artificial excess of energy happens at a very similar wavenumber for similar resolutions, it points to the fact that the transition from the inertial range to the dissipative range happens at the same scale for a given resolution and for all three codes. It is worth noting that in Fig. 4 we compare codes with a similar amount of *fluid elements*, which does not necessarily correspond to *same resolution*. In SPH codes, the spatial resolution is defined by the smoothing length, which covers significantly more than just one particle. At  $256^3$  cells, the spatial resolution of AREPO roughly corresponds to  $1/256 \sim 3.9 \times 10^{-3}$ , which is in fact similar to our  $400^3$  SPH simulation, which has an average smoothing length of  $h \sim 3.6 \times 10^{-3}$ . This means that if we compare at the same resolution, and according to the results of Fig. 4, SPH-EXA captures a considerably larger inertial range of the Kolmogorov cascade than AREPO. Likewise, the simulation of AREPO with  $512^3$  cells has an approximate resolution of  $\sim 1.9 \times 10^{-3}$ , which corresponds to our  $800^3$  simulation ( $h \sim 1.8 \times 10^{-3}$ ) represented with a dashed line in Fig. 4.

Figure 5 shows, from top to bottom, the module of the velocity, density, and enstrophy of the fluid at the end of our simulations. The two columns on the left are an excerpt of the results with AREPO and the SPH used in [9]. It is clear from these two columns that the SPH used in that work was not able to resolve subsonic turbulence, since it is missing all small-scale features. The two columns on the right show the results of SPH-EXA with  $250^3$  and  $1000^3$  particles. The similarities with the results of AREPO are evident, and there is a rich mix of fine structures that becomes richer with increasing resolution. This can also be seen in Fig. 3, which illustrates a slice of the module of the velocity field at  $t = 10$  for different resolutions.

Finally, Fig. 6 is a detailed image of a slice of the module of velocity of the  $3000^3$  simulation where we can appreciate

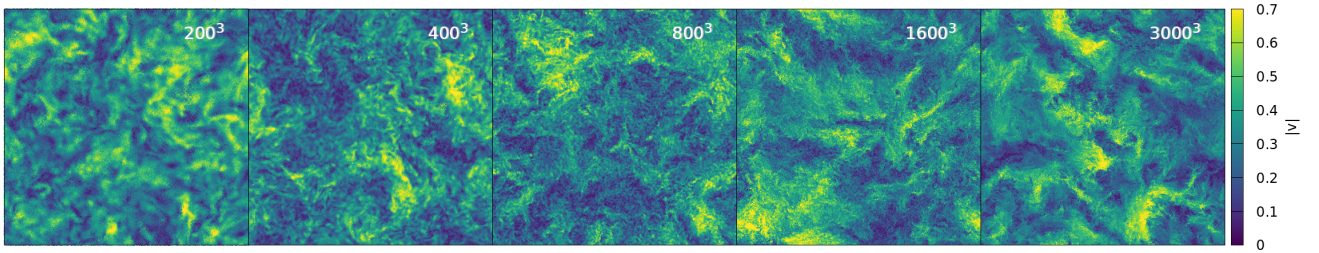


Fig. 3. Slice of the module of the velocity field with increasing resolution and calculated with SPH-EXA.

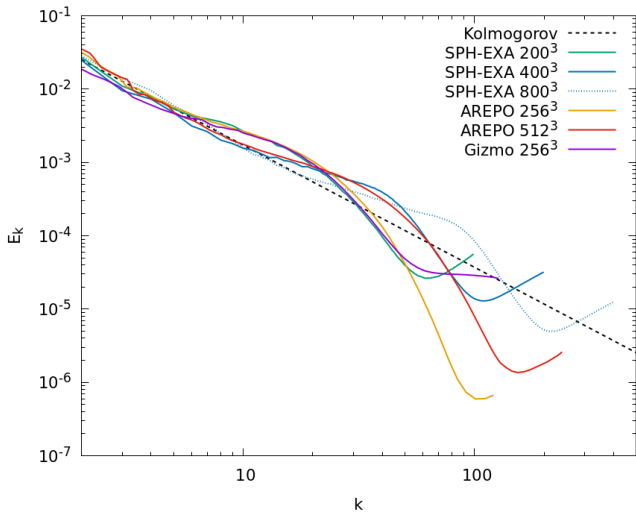


Fig. 4. Comparison of the power spectra of the velocity field for  $M = 0.3$  for different codes. AREPO [9] and GIZMO [20] curves are from their respective papers.

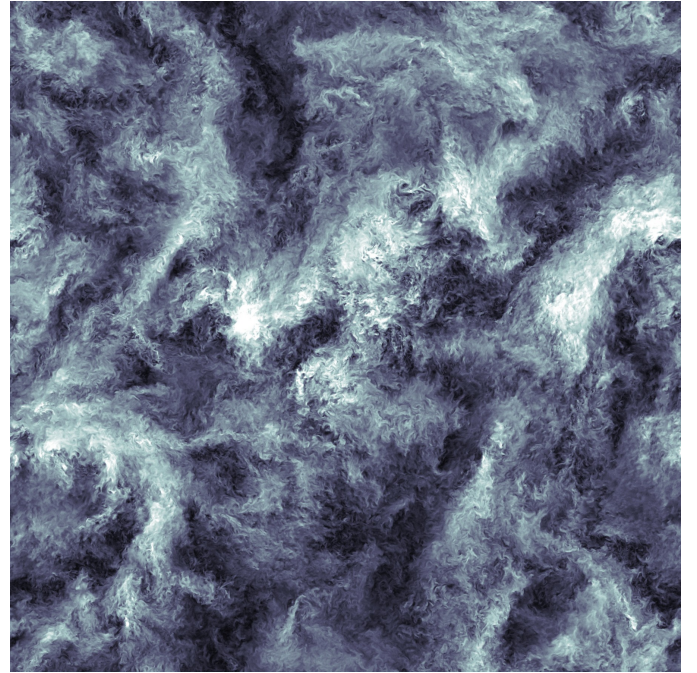


Fig. 6. Slice of the module of the velocity field at  $t = 10$  for a simulation with  $3000^3$  particles. Color follows the same scale as Fig. 3 but in grey.

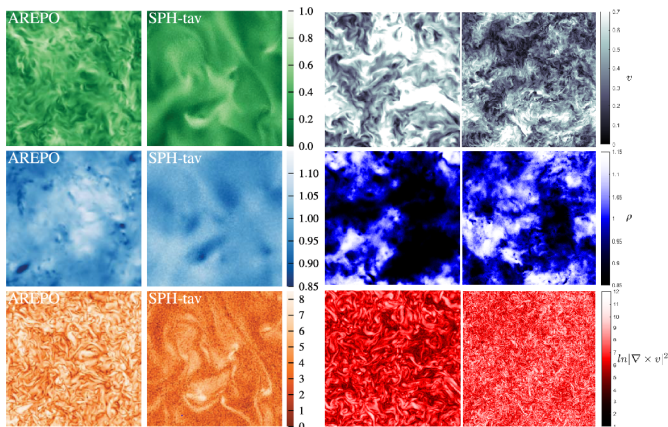


Fig. 5. Comparison of SPH-EXA results with AREPO and SPH-tav in [9]. From top to bottom: module of velocity, density, and enstrophy. The two columns on the left are an excerpt of the original results of AREPO and their SPH with reduced artificial viscosity (both with  $256^3$  fluid elements) of [9] shown in their Fig. 4. The two columns on the right are the results of SPH-EXA with  $250^3$  and  $1000^3$

the very small-scale features resolved with SPH-EXA.

#### IV. SUMMARY AND CONCLUSIONS

SPH has matured enough to be competitive in simulations of subsonic turbulence, obtaining results comparable to Eulerian codes. In particular, SPH-EXA combines a modern SPH formulation with the latest techniques in parallelization and the use of accelerators. This allowed us to overcome historical limitations of SPH, such as excessive dissipation and inaccurate gradient evaluations, which have traditionally prevented SPH from matching the performance of grid-based and moving-mesh codes in this field. Our findings not only align well with results from non-Lagrangian codes like AREPO and GIZMO, but also illustrate the robustness of SPH in handling complex turbulent flows at resolutions previously thought unattainable with this method.

We demonstrated that incorporating various components that address problems at multiple simulation scales collectively

achieves these results. Isolated enhancements in the SPH framework cannot tackle the subsonic turbulence; however, a synergy of these improvements can. In particular, our combination of an integral approach to derivatives, generalized volume elements, artificial viscosity switches, and artificial viscosity cleaner shows excellent results.

Finally, we proved that the inertial range of the power spectra significantly spans over larger wavenumbers with increasing resolution, exhibiting the same features as other non-Lagrangian state-of-the-art codes. These improvements have allowed SPH to finally tap into its inherent advantages, such as its intrinsic Lagrangian nature, excellent conservation properties, and adaptability to varied physical scenarios, thus paving the way for its application in more demanding astrophysical contexts.

#### ACKNOWLEDGMENT

This work has been supported by the Swiss Platform for Advanced Scientific Computing (PASC) project "SPH-EXA: Optimizing Smoothed Particle Hydrodynamics for Exascale Computing". It has also been carried out as part of the SKACH consortium through funding from SERI and supported by the Spanish MINECO grant PID2020-117252GB-I00 and by the AGAUR/Generalitat de Catalunya grant SGR-386/2021. We also acknowledge the financial support of the European Research Council through the ERC Synergy Grant "ECOGAL" (project ID 855130), from the German Excellence Strategy via the Heidelberg Cluster of Excellence (EXC 2181 - 390900948) "STRUCTURES", and from the German Ministry for Economic Affairs and Climate Action in project "MAINN" (funding ID 50002206). The numerical calculations have been supported by the EuroHPC-JU Extreme Scale Access Mode through the project "TGSF: The role of turbulence and gravity in star formation: unveiling the sonic scale with Smoothed Particle Hydrodynamics" (proposal ID: EHPC-EXT-2023E01-031). The authors acknowledge the support of the LUMI Supercomputer Center, the Swiss National Supercomputing Center (CSCS - allocation c32), and the Center for Scientific Computing (sciCORE) at the University of Basel, where these calculations were performed.

#### REFERENCES

- [1] L. B. Lucy, "A numerical approach to the testing of the fission hypothesis." *The Astronomical Journal*, vol. 82, pp. 1013–1024, Dec. 1977, publisher: IOP ADS Bibcode: 1977AJ.....82.1013L.
- [2] R. A. Gingold and J. J. Monaghan, "Smoothed particle hydrodynamics: theory and application to non-spherical stars." *Monthly Notices of the Royal Astronomical Society*, vol. 181, pp. 375–389, Nov. 1977, publisher: OUP ADS Bibcode: 1977MNRAS.181..375G.
- [3] M. B. Liu and G. R. Liu, "Smoothed Particle Hydrodynamics (SPH): an Overview and Recent Developments," *Archives of Computational Methods in Engineering*, vol. 17, no. 1, pp. 25–76, Mar. 2010.
- [4] D. J. Price, "Smoothed particle hydrodynamics and magnetohydrodynamics," *Journal of Computational Physics*, vol. 231, no. 3, pp. 759–794, Feb. 2012.
- [5] J. J. Monaghan, "Smoothed Particle Hydrodynamics and Its Diverse Applications," *Annual Review of Fluid Mechanics*, vol. 44, no. Volume 44, 2012, pp. 323–346, Jan. 2012, publisher: Annual Reviews.
- [6] U. Frisch, *Turbulence. The legacy of A.N. Kolmogorov*, Jan. 1995, publication Title: Turbulence. The legacy of A. N. Kolmogorov ADS Bibcode: 1995tlan.book.....F.
- [7] A. Kolmogorov, "The Local Structure of Turbulence in Incompressible Viscous Fluid for Very Large Reynolds' Numbers," *Akademiia Nauk SSSR Doklady*, vol. 30, pp. 301–305, Jan. 1941, aDS Bibcode: 1941DoSSR..30..301K.
- [8] S. Kitsionas, C. Federrath, R. S. Klessen, W. Schmidt, D. J. Price, L. J. Dursi, M. Gritschneider, S. Walch, R. Piontek, J. Kim, A.-K. Jappsen, P. Ciecielag, and M.-M. M. Low, "Algorithmic comparisons of decaying, isothermal, supersonic turbulence," *Astronomy & Astrophysics*, vol. 508, no. 1, pp. 541–560, Dec. 2009, number: 1 Publisher: EDP Sciences.
- [9] A. Bauer and V. Springel, "Subsonic turbulence in smoothed particle hydrodynamics and moving-mesh simulations," *Monthly Notices of the Royal Astronomical Society*, vol. 423, no. 3, pp. 2558–2578, Jul. 2012, publisher: Oxford Academic.
- [10] K. Dolag, F. Vazza, G. Brunetti, and G. Tormen, "Turbulent gas motions in galaxy cluster simulations: the role of smoothed particle hydrodynamics viscosity," *Monthly Notices of the Royal Astronomical Society*, vol. 364, no. 3, pp. 753–772, Dec. 2005.
- [11] R. Valdarnini, "The impact of numerical viscosity in SPH simulations of galaxy clusters," *Astronomy & Astrophysics*, vol. 526, p. A158, Feb. 2011, publisher: EDP Sciences.
- [12] D. J. Price, "Resolving high Reynolds numbers in smoothed particle hydrodynamics simulations of subsonic turbulence," *Monthly Notices of the Royal Astronomical Society: Letters*, vol. 420, no. 1, pp. L33–L37, Feb. 2012.
- [13] A. Di Mascio, M. Antuono, A. Colagrossi, and S. Marrone, "Smoothed particle hydrodynamics method from a large eddy simulation perspective," *Physics of Fluids*, vol. 29, no. 3, p. 035102, Mar. 2017.
- [14] M. Antuono, S. Marrone, A. Di Mascio, and A. Colagrossi, "Smoothed particle hydrodynamics method from a large eddy simulation perspective. Generalization to a quasi-Lagrangian model," *Physics of Fluids*, vol. 33, no. 1, p. 015102, Jan. 2021.
- [15] R. Valdarnini, "Improved performances in subsonic flows of an sph scheme with gradients estimated using an integral approach," *The Astrophysical Journal*, vol. 831, no. 1, p. 103, Oct. 2016.
- [16] D. García-Senz, R. M. Cabezón, and J. A. Escartín,

- “Improving smoothed particle hydrodynamics with an integral approach to calculating gradients,” *Astronomy & Astrophysics*, vol. 538, p. A9, Feb. 2012.
- [17] R. M. Cabezón, D. García-Senz, and J. Figueira, “SPH-YNX: an accurate density-based SPH method for astrophysical applications,” *Astronomy & Astrophysics*, vol. 606, p. A78, Oct. 2017.
- [18] D. García-Senz, R. M. Cabezón, and J. A. Escartín, “Conservative, density-based smoothed particle hydrodynamics with improved partition of the unity and better estimation of gradients,” *Astronomy & Astrophysics*, vol. 659, p. A175, Mar. 2022.
- [19] N. Frontiere, C. D. Raskin, and J. M. Owen, “CRKSPH – A Conservative Reproducing Kernel Smoothed Particle Hydrodynamics Scheme,” *Journal of Computational Physics*, vol. 332, pp. 160–209, Mar. 2017.
- [20] P. F. Hopkins, “A new class of accurate, mesh-free hydrodynamic simulation methods,” *Monthly Notices of the Royal Astronomical Society*, vol. 450, no. 1, pp. 53–110, Jun. 2015.
- [21] V. Springel, “E pur si muove: Galilean-invariant cosmological hydrodynamical simulations on a moving mesh,” *Monthly Notices of the Royal Astronomical Society*, vol. 401, no. 2, pp. 791–851, Jan. 2010.
- [22] R. M. Cabezón, D. García-Senz, and J. A. Escartín, “Testing the concept of integral approach to derivatives within the smoothed particle hydrodynamics technique in astrophysical scenarios,” *Astronomy & Astrophysics*, vol. 545, p. A112, Sep. 2012.
- [23] J. I. Read and T. Hayfield, “SPHS: smoothed particle hydrodynamics with a higher order dissipation switch,” *Monthly Notices of the Royal Astronomical Society*, vol. 422, no. 4, pp. 3037–3055, Jun. 2012.
- [24] L. Cullen and W. Dehnen, “Inviscid smoothed particle hydrodynamics: Inviscid smoothed particle hydrodynamics,” *Monthly Notices of the Royal Astronomical Society*, vol. 408, no. 2, pp. 669–683, Oct. 2010.
- [25] T. R. Saitoh and J. Makino, “A density-independent formulation of smoothed particle hydrodynamics,” *The Astrophysical Journal*, vol. 768, no. 1, p. 44, Apr. 2013.
- [26] P. F. Hopkins, “A general class of Lagrangian smoothed particle hydrodynamics methods and implications for fluid mixing problems,” *Monthly Notices of the Royal Astronomical Society*, vol. 428, no. 4, pp. 2840–2856, Feb. 2013.
- [27] B. W. Ritchie and P. A. Thomas, “Multiphase smoothed-particle hydrodynamics,” *Monthly Notices of the Royal Astronomical Society*, vol. 323, no. 3, pp. 743–756, May 2001.
- [28] J. I. Read, T. Hayfield, and O. Agertz, “Resolving mixing in smoothed particle hydrodynamics,” *Monthly Notices of the Royal Astronomical Society*, vol. 405, no. 3, pp. 1513–1530, Jul. 2010.
- [29] R. M. Cabezón, D. García-Senz, and A. Relaño, “A one-parameter family of interpolating kernels for smoothed particle hydrodynamics studies,” *Journal of Computational Physics*, vol. 227, no. 19, pp. 8523–8540, Oct. 2008.
- [30] R. M. Cabezón and D. García-Senz, “Mixing Sinc kernels to improve interpolations in smoothed particle hydrodynamics without pairing instability,” *Monthly Notices of the Royal Astronomical Society*, vol. 528, no. 2, pp. 3782–3796, Feb. 2024.
- [31] W. Dehnen and H. Aly, “Improving convergence in smoothed particle hydrodynamics simulations without pairing instability,” *Monthly Notices of the Royal Astronomical Society*, vol. 425, no. 2, pp. 1068–1082, Sep. 2012.
- [32] H. Wendland, “Piecewise polynomial, positive definite and compactly supported radial functions of minimal degree,” *Advances in Computational Mathematics*, vol. 4, no. 1, pp. 389–396, Dec. 1995.
- [33] A. Arth, J. Donnert, U. Steinwandel, L. Böss, T. Halbesma, M. Pütz, D. Hubber, and K. Dolag, “WVTICs – SPH initial conditions for everyone,” *arXiv e-prints*, p. arXiv:1907.11250, Jul. 2019.
- [34] G. E. Uhlenbeck and L. S. Ornstein, “On the theory of the brownian motion,” *Phys. Rev.*, vol. 36, pp. 823–841, Sep 1930. [Online]. Available: <https://link.aps.org/doi/10.1103/PhysRev.36.823>
- [35] C. Federrath, J. Roman-Duval, R. S. Klessen, W. Schmidt, and M. M. Mac Low, “Comparing the statistics of interstellar turbulence in simulations and observations. Solenoidal versus compressive turbulence forcing,” *Astronomy & Astrophysics*, vol. 512, p. A81, Mar. 2010.

(used to reserve space for the reference number labels box)